Journal of Fluids and Structures (1998) **12,** 335–351

THE INFLUENCE OF SHAPE ON THE RAYLEIGH CONDUCTIVITY OF A WALL APERTURE IN THE PRESENCE OF GRAZING FLOW

S. M. GRACE, K. P. HORAN AND M. S. HOWE

Department of Aerospace and Mechanical Engineering, Boston University
110 Cummington Street, Boston, MA 02215, U.S.A.

(Received 22 April 1997 and accepted in revised form 18 December 1997)

A numerical investigation of the influence of grazing flow on the Rayleigh conductivity K_R of an aperture in a thin rigid wall is made. The Mach number is sufficiently small for the local motion near the aperture to be regarded as incompressible, and the Reynolds number is taken to be large enough for the aperture shear layer to be modelled by a vortex sheet. The vortex sheet is assumed to be linearly perturbed from its equilibrium position by a small amplitude, time-harmonic pressure, and K_R is determined from the ratio of the resulting aperture volume flux to the applied pressure. The frequency dependence of K_R is computed for a variety of aperture shapes for both one-sided and two-sided flows. For apertures of equal maximum streamwise dimension in one-sided flow, the Strouhal number range within which perturbation energy is extracted from the mean flow [where $\mathscr{I}m(K_R) > 0$] is found to be effectively independent of the aperture shape. The frequency of the first "operating stage" of self-sustained (*unforced*) oscillations of the aperture shear layer lies approximately in the center of this range, and is the minimum frequency at which narrow band sound is generated by nominally steady flow over the aperture. The numerical predictions are shown to satisfy the reverse flow reciprocal theorem, according to which K_R is unchanged when the mean flow directions on both sides of the wall are reversed (when vortex shedding occurs from the "opposite" edge of the aperture).

1. INTRODUCTION

A TIME HARMONIC PRESSURE LOAD $(p_0^+ - p_0^-)\mathrm{e}^{-\mathrm{i}\omega t}$ is applied across an aperture in a thin rigid wall, which coincides with the plane $x_2 = 0$ of the rectangular coordinate system (x_1, x_2, x_3) (see Figure 1). The pressures $p_0^+ - p_0^-$ are uniform, respectively, in $x \gtrless 0$, and produce a volume flow through aperture in the positive x_2-direction equal to $Q\mathrm{e}^{-\mathrm{i}\omega t}$.

The *Rayleigh conductivity* is defined in terms of these quantities by the ratio (Rayleigh 1945).

$$K_R(\omega) = \frac{\mathrm{i}\omega\rho_0 Q}{p_0^+ - p_0^-}, \tag{1.1}$$

where ρ_0 is the mean fluid density, which is assumed to be constant. Conductivity has the dimensions of length; for an ideal, incompressible fluid (in the absence of mean flow) its value is entirely determined by the geometric shape of the aperture, being equal to $2R$ for a circular aperture of radius R, and approximately equal to $2 \times \sqrt{(\text{aperture area}/\pi)}$ for an arbitrary, nonelongated aperture. In a real fluid, K_R is generally a complex function of the

0889-9746/98/030335 + 17 $25.00/fl970145

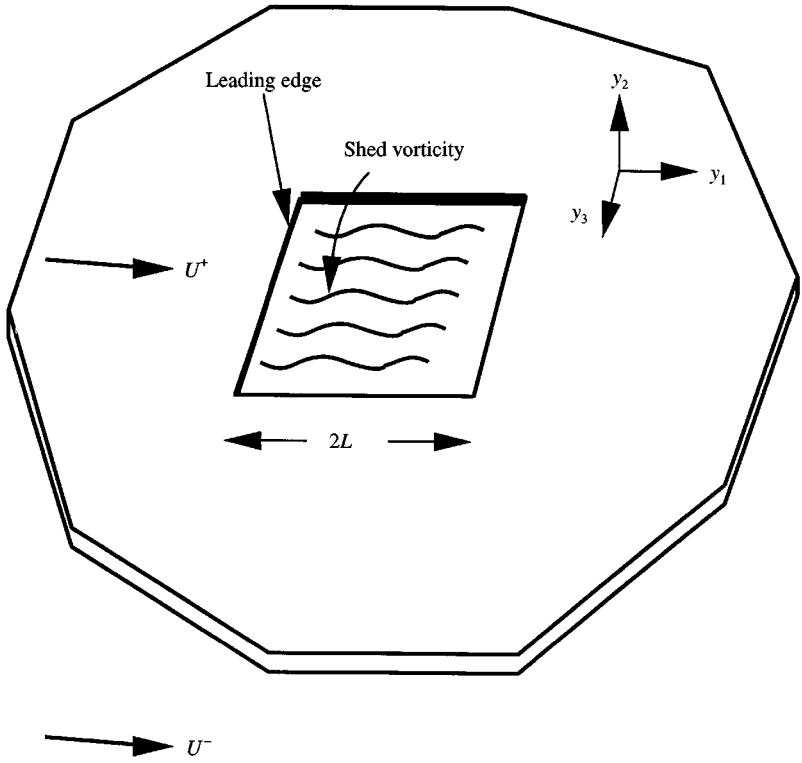

Figure 1. Grazing flow past a wall aperture.

frequency ω, and energy of the applied pressure field (an incident sound wave, for example) is dissipated in the aperture at a rate

$$\Pi = -\frac{1}{2}\mathscr{R}e(Q^*[p_0^+ - p_0^-]) \equiv -\frac{\mathscr{I}m\{K_R(\omega)\}}{2\rho_0\omega}|p_0^+ - p_0^-|^2, \tag{1.2}$$

where the asterisk denotes the complex conjugate (Pierce 1989). The damping is *negative* ($\Pi < 0$) if $\mathscr{I}m\{K_R(\omega)\} > 0$ (for $\omega > 0$), which can happen in the presence of mean flow over one or both sides of the wall. The forced motion in the aperture then grows at the expense of mean flow kinetic energy (Howe *et al.* 1996) via coupling facilitated by unsteady vortex shedding from the aperture leading edge. The phase of the interaction of this vorticity with the trailing edge (after convection across the aperture) determines whether or not perturbation energy is extracted from or ceded to the mean flow.

The negative damping of forced motion in the presence of flow is related to the instability of the mean shear layer in the aperture (Lamb 1932) and to the possible occurrence of self-sustained oscillations that produce narrow band sound (Rossiter 1964; Rockwell 1983; Blake & Powell 1986; Howe *et al.* 1996). Such oscillations are maintained by feedback, involving the periodic generation of pressure "waves" at the trailing edge by interaction with shed vorticity, which triggers the cyclic formation of new vorticity at the leading edge. The oscillations are reinforced and sustained for a set of discrete value of the Strouhal number based on the streamwise length of the aperture and the mean flow velocity (Powell

1961; Rossiter 1964; Blake & Powell 1986). A quantitative understanding of the feedback mechanism is desirable because of its importance in a diverse range of physical systems including, for example, perforated baffles in heat exchangers, depressions in submarine and ship hulls, computer boards with closely spaced chip carriers, aircraft control surfaces and fuselage openings, and flow-through resonators of automobile mufflers.

To obtain a complete picture of the motion produced by the applied pressure, or of the frequency and amplitude of the self-sustaining oscillations, it is necessary to solve the nonlinear Navier–Stokes equations. However, an accurate first approximation to the forced motion and to the *frequencies* of self-sustained oscillations is furnished by a *linearized* treatment of the shear layer motion (Howe 1997*a*). This is because both the feedback and nonresonant energy transfers are governed primarily by the convection speed of vorticity across the aperture, which experiment shows to be essentially independent of the amplitude of the shear layer motion (Powell 1961; Holger, *et al.* 1977; Rockwell 1983; Blake & Powell 1986).

Approximations of this kind have been considered by Howe (1981*a*, *b*) for slot-type apertures of very large aspect ratio. The Reynolds number was taken to be sufficiently large that turbulence-free mean streams over the wall could be regarded as uniform, and the mean shear layer in the aperture was modelled by a vortex sheet that is *linearly* disturbed from its mean position. The same method was applied by Scott (1995) [see also Howe *et al.* (1996)] to a circular aperture, and by Howe (1997*a*, *c*) to rectangular apertures of arbitrary aspect ratio. The mean flow Mach number was assumed to be small enough for the aperture motion to be regarded as incompressible. Viscosity was ignored, except for its role in shedding vorticity from the leading edge of the aperture, which was incorporated by application of the Kutta condition. Howe (1997*a*) showed that linear theory predicts that $K_R(\omega)$ has simple poles in $\mathscr{I}m\,\omega > 0$, and that the real part of the complex frequency at a pole corresponds to the frequency of an "operating stage" of the self-sustained oscillations.

In this paper, the numerical method of Scott (1995) is extended to determine the effect of shape on the conductivity of an aperture in a thin wall in the presence of grazing flow. Detailed comparisons are made of the conductivities for shapes including the circle, square, triangle, "cross", and a square whose leading or trailing edge has triangular serrations ("crown"). When the Strouhal number, $\omega L/U$, is defined in terms of the maximum streamwise dimension $2L$ of the aperture and a mean flow velocity U, it is shown that aperture shape has effectively no influence on the Strouhal number ranges in which forced oscillations are unstable [i.e., where $\Pi(\omega)$ of equation (1.2) is *negative*]. According to Howe (1997*c*) this indicates that the minimum Strouhal number of self-sustained oscillations (i.e., of the first operating stage) does not vary significantly with geometry. The calculations also furnish direct numerical confirmation of *reverse flow reciprocity* (Howe *et al.* 1996), namely, that the value of $K_R(\omega)$ is unchanged when the direction of the mean flow is reversed. This remarkable theorem implies, for example, that the conductivity of a square aperture with a serrated leading edge is unchanged when the flow is reversed, such that shed vorticity from a straight leading edge now *impinges* on the serrations. This result could be important in assessing the efficiency of "spoilers" intended to reduce the coherence of sound generated by vortex shedding.

The numerical problem is formulated in Section 2, and applied in Section 3 to determine the conductivities of apertures of various shapes in the presence of mean flow over one or both sides of the wall. A comparison is also made with the approximate theory of Howe (1997*a*). Reverse flow reciprocity is discussed in Section 4.

2. THE GOVERNING EQUATIONS

2.1. Equation of Motion of the Vortex Sheet

The motion on either side of the aperture induced by the perturbed motion of the vortex sheet is regarded as incompressible and irrotational, and is expressed in terms of velocity potentials $\Phi^{\pm}$, respectively, in the regions $x_2 \gtrless 0$ "above" and "below" the wall. The potentials satisfy the Laplace equation

$$\nabla^2 \Phi^{\pm} = 0, \qquad x_2 \gtrless 0, \tag{2.3}$$

and the associated pressure fluctuations $p^{\pm}$ are given by the linearized Euler equation in the form

$$p^{+} = \mathrm{i}\rho_0 \left(\omega + \mathrm{i}U^{+} \frac{\partial}{\partial x_1}\right) \Phi^{+}, \qquad x_2 > 0, \tag{2.4}$$

$$p^{-} = \mathrm{i}\rho_0 \left(\omega + \mathrm{i}U^{-} \frac{\partial}{\partial x_1}\right) \Phi^{-}, \qquad x_2 < 0, \tag{2.5}$$

The equation of motion of the vortex sheet is obtained by equating the net pressures on opposite sides at the undisturbed position of the sheet, i.e.,

$$p_0^{+} + \mathrm{i}\rho_0 \left(\omega + \mathrm{i}U^{+} \frac{\partial}{\partial x_1}\right) \Phi^{+} = p_0^{-} + \mathrm{i}\rho_0 \left(\omega + \mathrm{i}U^{-} \frac{\partial}{\partial x_1}\right) \Phi^{-}, \qquad x_2 = 0, \tag{2.6}$$

where the field point $(x_1, 0, x_3)$ lies within the aperture.

The solution of the Laplace equation (2.3) can be written as

$$\Phi^{\pm}(\mathbf{x}) = \mp \frac{1}{2\pi} \int_{-\infty}^{\infty} \int_{-\infty}^{\infty} \frac{\partial \Phi^{\pm}/\partial y_2}{|\mathbf{x} - \mathbf{y}|} \, \mathrm{d}y_1 \, \mathrm{d}y_2, \qquad \mathbf{y} = (y_1, 0, y_3), \qquad x_2 \gtrless 0, \tag{2.7}$$

where the normal derivatives $\partial \Phi^{\pm}/\partial y_2$ are evaluated on $y_2 = \pm 0$ (Hildebrand 1976). These derivatives are related to the displacement ζ of the vortex sheet (in the y_2 direction) by

$$\frac{\partial \Phi^{\pm}}{\partial y_2} = -\mathrm{i}\left(\omega + \mathrm{i}U^{\pm} \frac{\partial}{\partial y_1}\right) \zeta, \qquad y_2 = \pm 0,$$

which permits equation (2.6) to be cast in the form

$$\frac{p_0^{+} - p_0^{-}}{\rho_0} = \frac{1}{2\pi} \left[\left(\omega + \mathrm{i}U^{-} \frac{\partial}{\partial x_1}\right)^2 + \left(\omega + \mathrm{i}U^{+} \frac{\partial}{\partial x_1}\right)^2 \right] \int_S \frac{\zeta(y_1, y_3)}{|\mathbf{x} - \mathbf{y}|} \, \mathrm{d}y_1 \, \mathrm{d}y_3, \tag{2.8}$$

where the integration is now restricted to the aperture opening S.

This equation is simplified by introducing the nondimensional notation

$$\mathbf{X} = \mathbf{x}/L, \quad \mathbf{Y} = \mathbf{y}/L, \tag{2.9}$$

$$\sigma = \omega L/U^{+}, \qquad Z = \frac{\zeta \rho_0 \sigma^2 (U^{+})^2}{\pi L (p_0^{+} - p_0^{-})}, \tag{2.10, 2.11}$$

where σ is the Strouhal number and $2L$ is the maximum streamwise length of the aperture. By integrating equation (2.8) with respect to the second-order differential operator in x_1 on the right-hand side, we can then write

$$\int_S \frac{Z(Y_1, Y_3)}{|\mathbf{X} - \mathbf{Y}|} \, \mathrm{d}Y_1 \, \mathrm{d}Y_3 = 1 + \alpha(X_3) \mathrm{e}^{\mathrm{i}\sigma_1 X_1} + \beta(X_3) \mathrm{e}^{\mathrm{i}\sigma_2 X_1}, \qquad X_2 = 0. \tag{2.12}$$

Here, $\sigma_{1,2}$ are the nondimensional Kelvin–Helmholtz wave numbers (Lamb 1932):

$$\sigma_1 = \frac{\omega L(1+\mathrm{i})}{U^+ + \mathrm{i}U^-}, \qquad \sigma_2 = \frac{\omega L(1-\mathrm{i})}{U^+ - \mathrm{i}U^-}. \tag{2.13}$$

$\alpha(X_3)$ and $\beta(\mathrm{X}_3)$ are "constants" of integration that depend on the spanwise coordinate X_3. They may be interpreted as the amplitudes of instability waves of wave numbers $\sigma_{1,2}$ propagating across the aperture, their values being fixed by application of the Kutta condition at the leading edge (Scott 1995; Howe *et al.* 1996).

When the mean velocities are the same on both sides of the wall ($U^+ = U^-$) the wave numbers σ_1 and σ_2 are both equal to σ, and the right-hand side of equation (2.12) may be replaced by

$$1 + \alpha(X_3)\mathrm{e}^{\mathrm{i}\sigma X_1} + \beta(X_3)X_1\mathrm{e}^{\mathrm{i}\sigma X_1}.$$

2.2. The Numerical Procedure

Equation (2.12) is solved for the nondimensional displacement Z by introducing the Cartesian grid shown schematically in Figure 2 and discretizing the integration over the aperture. The displacement $Z(Y_1, Y_3)$ is taken to be constant and equal to Z_{ij} on the grid cell centred on (Y_{1i}, Y_{3j}), but the kernel function $1/|\mathbf{X} - \mathbf{Y}|$ is integrated analytically. The Kutta condition is imposed by setting $Z = 0$ on the first two grid cells in each grid row of constant Y_3 (indicated in the figure by the asterisks), i.e., by demanding that $Z_{1j} = Z_{2j} = 0$; this is equivalent to requiring that the displacement and streamwise derivative of the vortex sheet vanish at the aperture leading edge. When this is done, Z_{1j} and Z_{2j} may be discarded from the discretized equation of motion and their respective roles in the vector of unknowns assumed by the corresponding instability wave amplitudes $\alpha(Y_{3j})$ and $\beta(Y_{3j})$. The equation

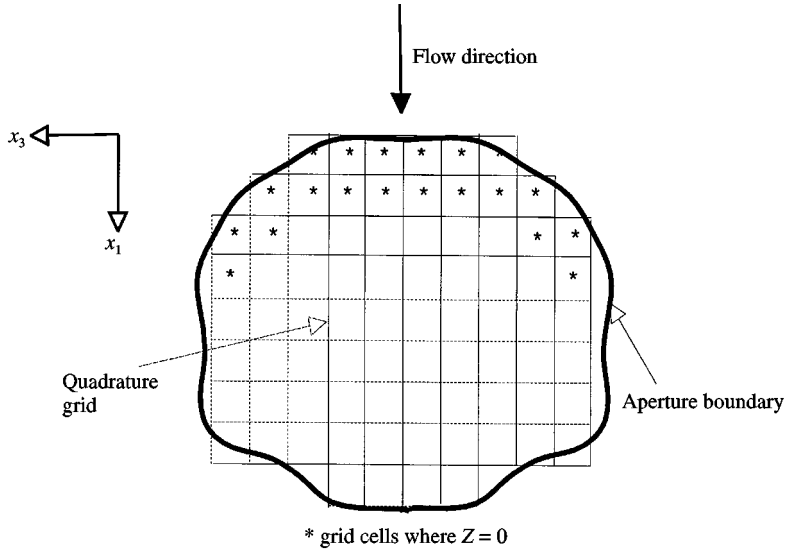

Figure 2. Quadrature grid used to solve the integral equation; asterisks denote the elements used to satisfy the Kutta condition.

is then solved for the Z_{ij} by collocation, by requiring it to be satisfied at each lattice point of the grid.

Definition (1.1) and the solution array Z_{ij} then determine the Rayleigh conductivity by

$$K_R(\omega) = \pi L \iint_S Z(Y_1, Y_3)\,\mathrm{d}Y_1\,\mathrm{d}Y_3 \approx \pi L \sum_{i \neq 1,2;\, j} Z_{ij} W_{ij}, \tag{2.14}$$

where W_{ij} denotes the area of the grid element centred on (Y_{1i}, Y_{3j}).

3. NUMERICAL RESULTS

The set of aperture shapes considered in this investigation is illustrated in Figure 3, and includes the circle, square, cross, two different forward (upstream pointing) and backward (downstream pointing) facing triangles, and a "crown" (square with triangular serrated leading or trailing edge). For each aperture, the conductivity is calculated in the normalized form

$$K_R(\omega)/2L = \Gamma - \mathrm{i}\Delta,$$

for both one-sided flow (where $U^- = 0$), and for two-sided flow when $U^+ = U^-$.

The circular aperture was treated by Scott (1995), and his results have been used as one method to validate the integration procedure. Chanaud (1994) discussed the cross-shaped

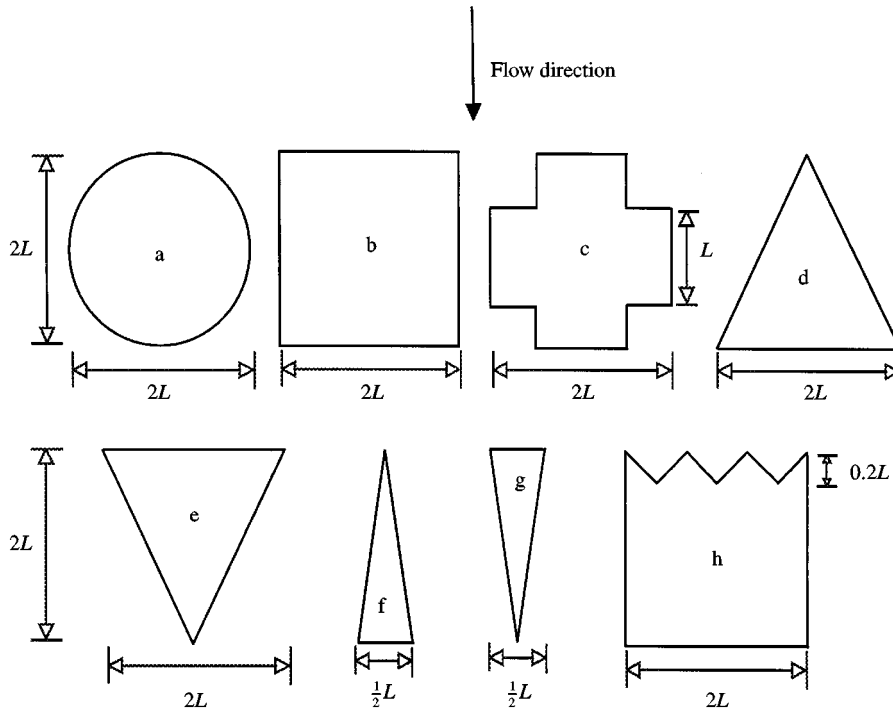

Figure 3. Aperture cross-sections studied: (a) circle; (b) square; (c) cross; (d) forward pointing triangle; (e) backward pointing triangle; (f) smaller forward pointing triangle; (g) smaller backward pointing triangle; (h) crown.

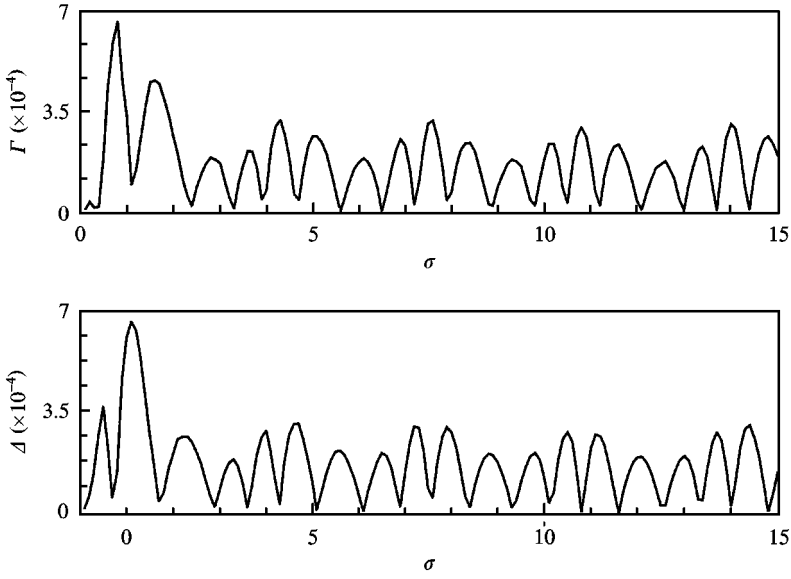

Figure 4. Effect of single precision versus double-precision numerical calculations.

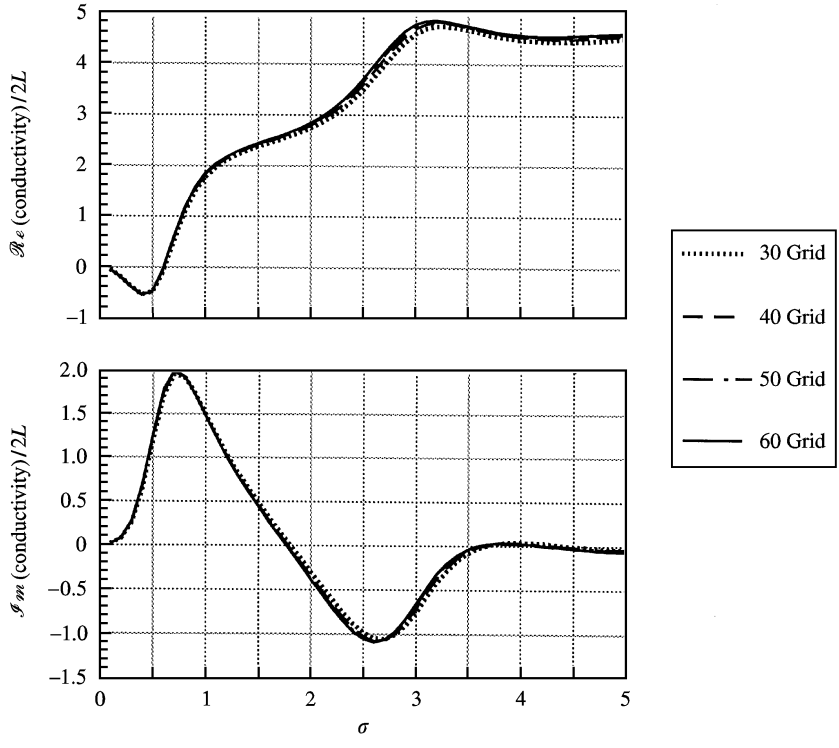

Figure 5. Dependence of Rayleigh conductivity calculation on grid resolution. One-sided grazing flow past a square aperture.

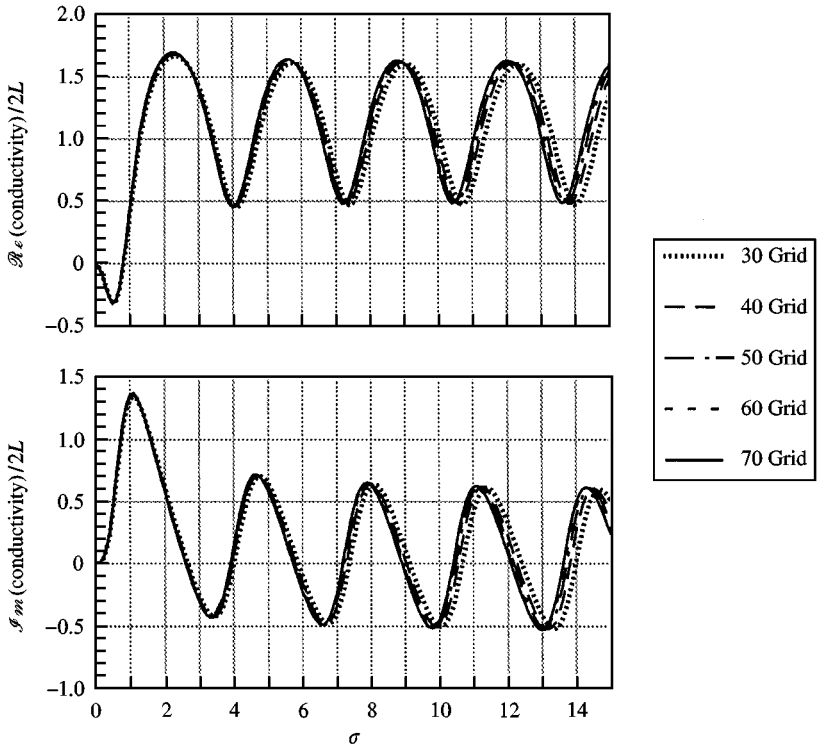

Figure 6. Dependence of Rayleigh conductivity calculation on grid resolution. Two-sided grazing flow past a square aperture.

aperture in the absence of flow. The "crown" is examined because of its relevance to applications in which it is desirable to create incoherent streams of vorticity by shedding from a serrated edge. The computations are performed in single precision using a square mesh discretization of equation (2.12). The validity of using single precision was tested by calculating the conductivity for two-sided flow past a square aperture using both single and double precision and comparing the results. The absolute difference between the real part of the conductivity from the two calculations and the absolute difference between the imaginary part from the two calculations are plotted in Figure 4. The maximum difference is 7×10^{-4} and the average absolute difference is approximately 2×10^{-4}. As this difference is so small, there is no loss of information when performing the calculation using single precision.

The size of the square mesh elements is set by choosing the number of mesh elements stretching between the leading and trailing edges along the centreline of the aperture. Figures 5 and 6 show the effect of increasing the mesh density on the calculations of the conductivity for one and two sided grazing flow past a square aperture. (When the number of elements increases from 30 to 60, this decreases the grid element nondimensional area from $4{\cdot}4 \times 10^{-3}$ to $1{\cdot}1 \times 10^{-3}$.) In these figures the calculated real and imaginary components, Γ and Δ, of the conductivities for one-sided and two-sided flow are plotted against Strouhal number $\sigma = \omega L/U$. Figure 5 shows that, for the Strouhal numbers of interest in the one-sided flow case, the numerical results become completely grid independent at a grid

corresponding to 50 mesh elements in the streamwise direction. The two-sided flow case, which can be calculated to a higher Strouhal number, is grid independent for Strouhal numbers less than 10 when the grid has 60 elements in the streamwise direction.

For the cases of both one-sided and two-sided flow, the difference between the discretizations of 40, 50 and 60 elements are very small. Past a Strouhal number of 10, a grid of more than 70 elements must be used as the finer grids shift the results for the higher Strouhal number of the left slightly. Because our objective is to compare the conductivity for several aperture shapes, we have used a discretization of 40. The small phase shift that exists at the higher Strouhal numbers will be the same for all of the calculations and was a small trade-off for a large speed-up computationally. If a discretization higher than 40 was used for a specific case, it will be noted.

3.1. One-sided Mean Flow

The real and imaginary components, Γ and Δ, of the conductivities for one-sided flow past the different aperture shapes are plotted against Strouhal number σ in Figure 7. All of these plots are qualitatively the same. In particular, $\Delta > 0$ at low frequencies, so that forced motion of the aperture at such frequencies is always damped [see equation (1.2)], the energy of the applied pressure force (produced by an incident sound wave, for example) being lost to the mean flow. The damping is negative ($\Delta < 0$) over a band of higher frequencies, wherein the mean flow releases kinetic energy when shed vorticity interacts with the aperture trailing edge. In this case there would be a net gain in acoustic energy when the shear layer is excited by sound. By invoking function theoretic arguments it can be shown (Howe 1997*c*) that $K_R(\omega)$ has a simple pole at a complex frequency in the upper half-plane whose real part is approximately equal to the real frequency at which $\Delta(\omega)$ is a minimum. The real part of the frequency at this pole corresponds to the Strouhal number of the first operating stage of self-sustained oscillations of the aperture shear layer (Howe 1997*a*). It is only weakly dependent on aperture shape, since all the minima in Figure 7 lie within the interval $2{\cdot}5 < \omega L/U < 3{\cdot}2$. In particular, the conductivity of the square aperture with a serrated leading edge (the "crown") is practically the same as that for the straight-edged square. A comparison of the conductivities for the forward and backward facing triangles indicates that $K_R(\omega)$ is unchanged when the flow direction is reversed. This reverse flow reciprocity is further discussed, below. The calculation of the conductivity of the smaller triangle required a mesh with 100 elements in the streamwise direction.

In the absence of flow, Rayleigh (1945) showed that $K_R\sqrt{A} \approx$ constant, where A is the aperture area. The result of normalizing $K_R(\omega)$ in the same way in the presence of one-sided flow is shown in Figures 8 and 9.

3.2. Uniform Two-sided Mean Flow, $U^+ = U^-$

Figure 10 shows the calculated frequency dependency of Γ and Δ when the mean flow speed is the mean on both sides and equal to U. The quasi-periodic behavior of these functions confirms the earlier prediction of Scott (1995) for the circle. In this case, however, the aperture motions are only conditionally unstable, in the sense that an incident perturbation will grow by extracting energy from the mean flow provided $\Delta < 0$, but there are no poles in $\mathscr{I}m(\omega) > 0$, so that self-sustaining oscillations are not possible, at least in the ideal limit of a vanishingly thin wall (Howe 1997*c*). The minima of Δ occur at roughly the same values

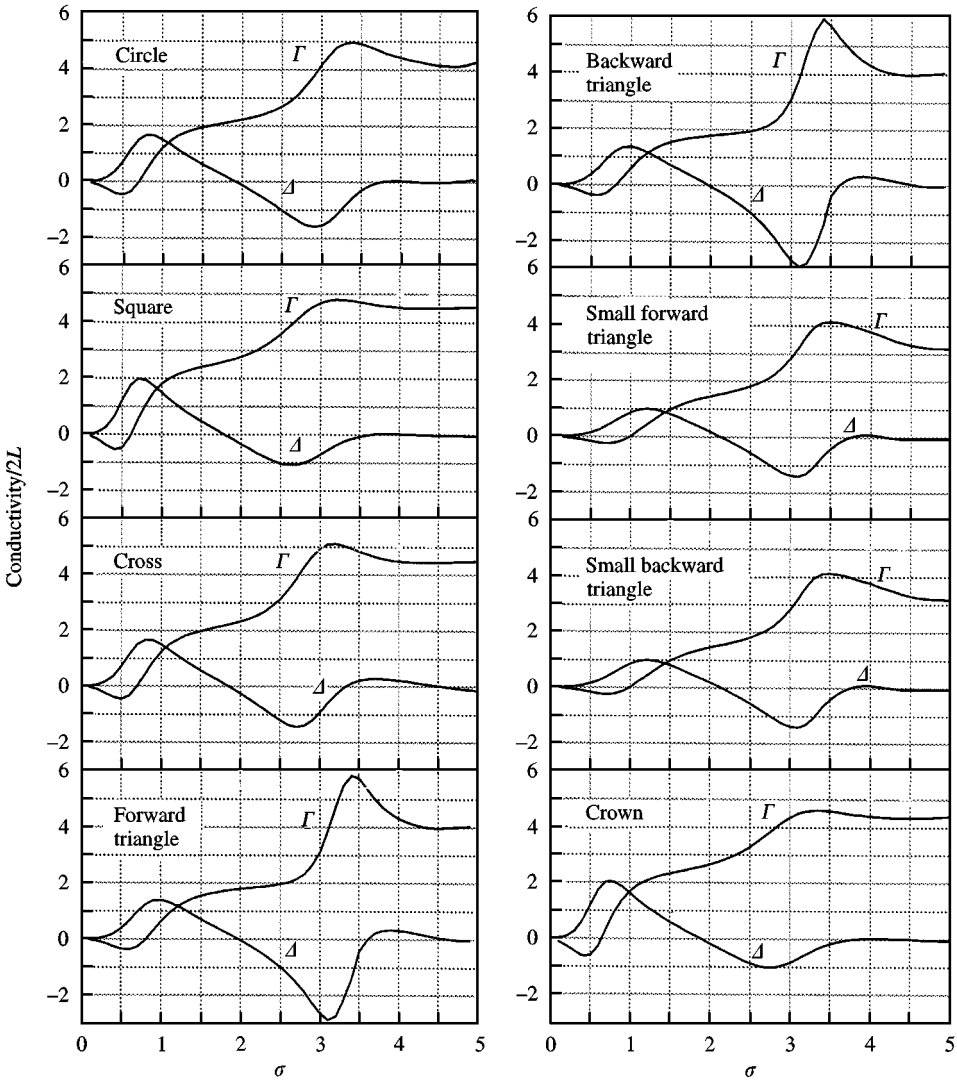

Figure 7. The Rayleigh conductivity for one-sided grazing flow past aperture with shapes: circle, square, cross, forward triangle, backward triangle, small forward triangle, small backward triangle, and crown.

of σ for all the cases shown in the figures; this is also evident from Figures 11 and 12, where the conductivities are normalized with respect to $\sqrt{A}$. Again, the agreement shown in Figure 12 for corresponding forward and backward triangles is in accord with reverse flow reciprocity.

For regularly shaped apertures such as the square, the results indicate that $K_R(\omega)$ is periodic at high enough frequency, and that the magnitudes of successive maxima and minima are effectively constant. For those apertures whose streamwise dimension decreases continuously with distance from the line of symmetry (the circle and triangle), the magnitudes of successive maxima and minima decrease with increasing σ. For the cross-shaped

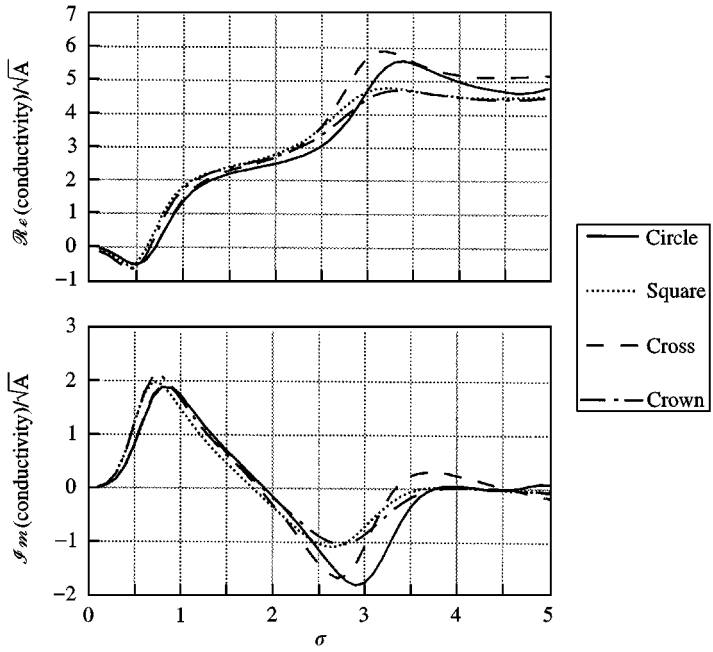

Figure 8. Real part (top) and imaginary part (bottom) of the Rayleigh conductivity normalized by the square root of the area for circle, square, cross, and crown apertures with flow on one side.

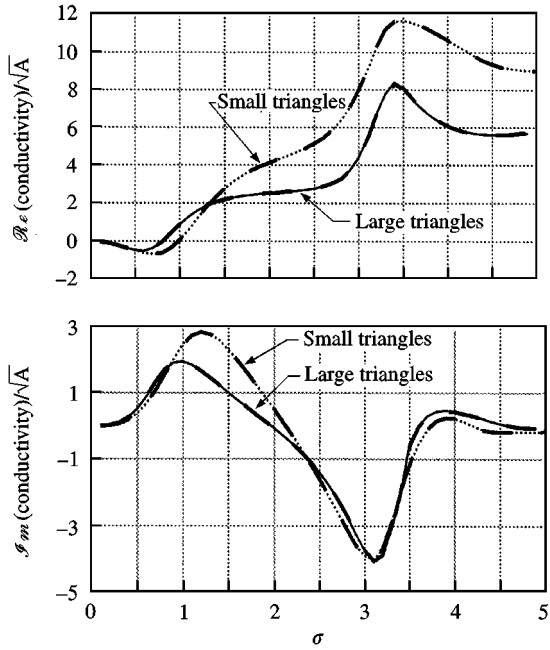

Figure 9. Real part (top) and imaginary part (bottom) of the Rayleigh conductivity normalized by the square root of the area for the large and small, forward and backward facing triangle apertures with flow on one side. Thick dashed lines represent results for the forward facing triangles.

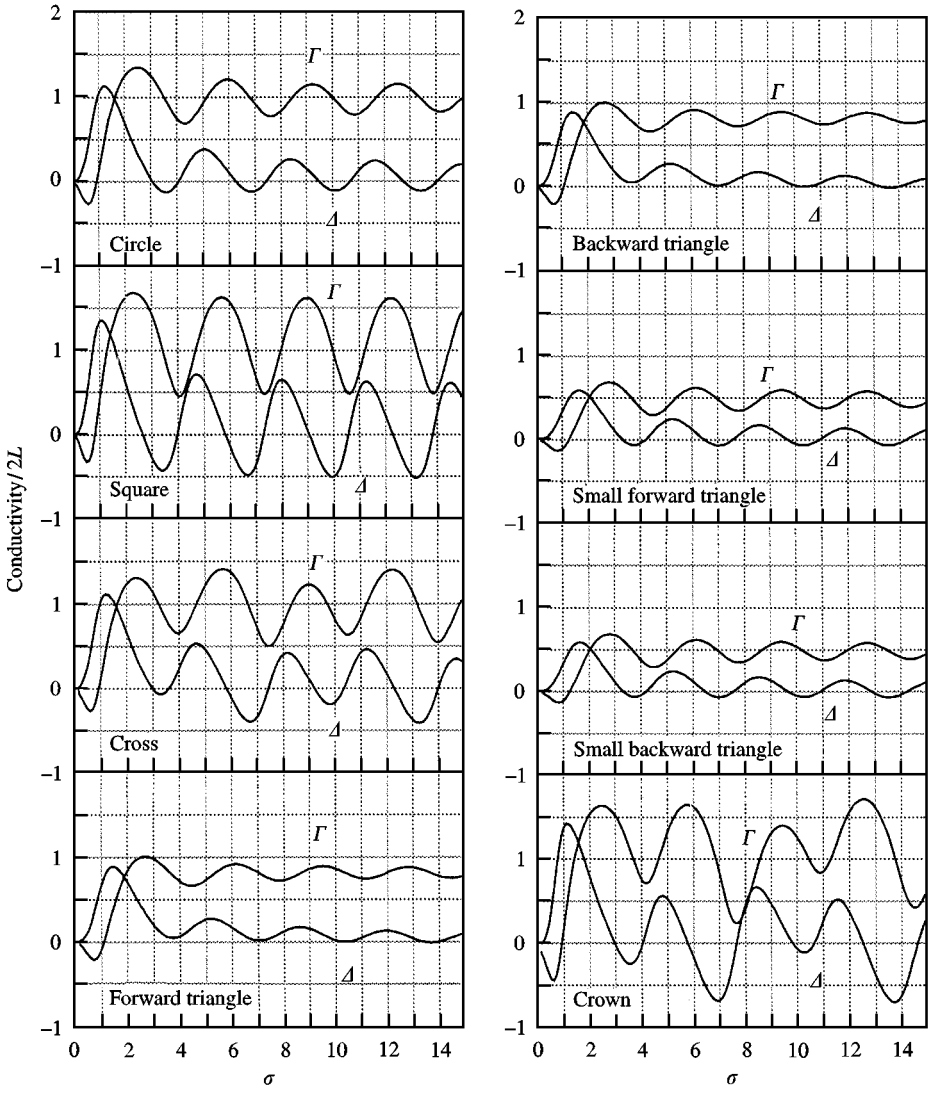

Figure 10. The Rayleigh conductivity for equal two-sided grazing flow past apertures with shapes: circle, square, cross forward triangle, backward triangle, small forward triangle, small backward triangle and crown.

aperture, which has two very different streamwise length scales, successive maxima and minima exhibit two distinct values which recur alternately as the frequency increases. In the case of the "crown" shaped aperture, there are two dominant length scales, which are reflected in the two alternating sets of values for the maxima and minima, in addition however, the magnitudes of the peaks gradually decrease with increasing σ.

3.3. One-dimensional Approximation to the Aperture Motion

Howe (1997*b*) has estimated the influence of mean flow on the conductivity of *rectangular* apertures (with sides parallel to the mean flow direction) by neglecting the dependence of

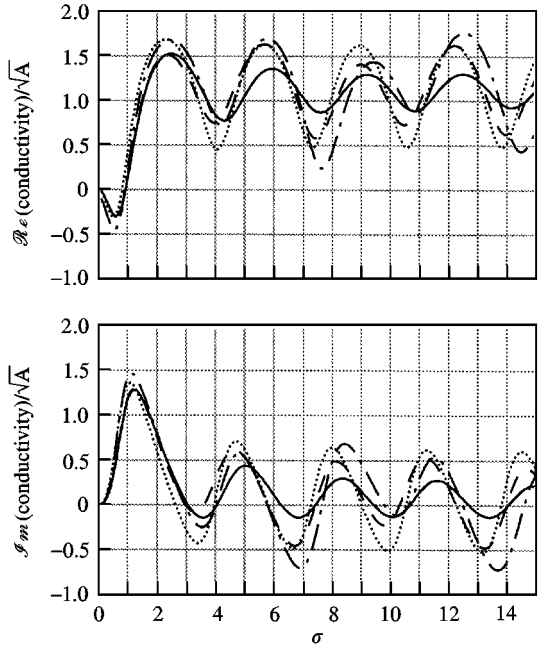

Figure 11. Real part (top) and imaginary part (bottom) of real Rayleigh conductivity normalized by the square root of the area for circle, square, cross, and crown apertures with equal flow on both faces: ——, circle; ⋯, square; – – cross; — – —, crown.

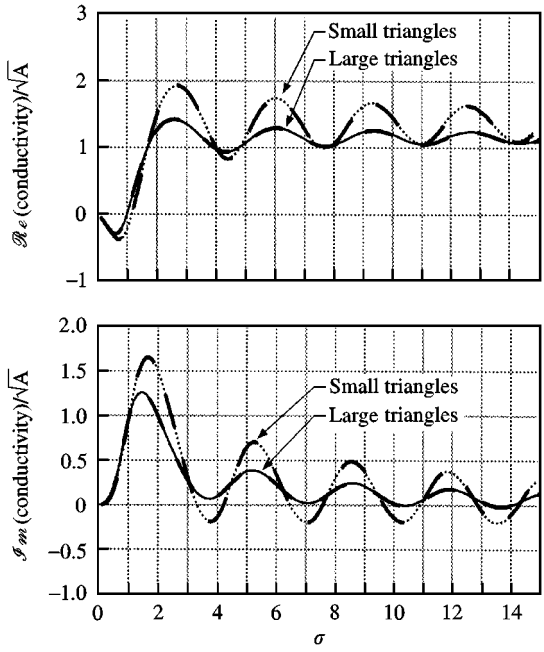

Figure 12. Real part (top) and imaginary part (bottom) of the Rayleigh conductivity normalized by the square root of the area for the large and small, forward and backward facing triangle apertures with equal flow on both faces. Thick dashed lines represent results for the forward facing triangle.

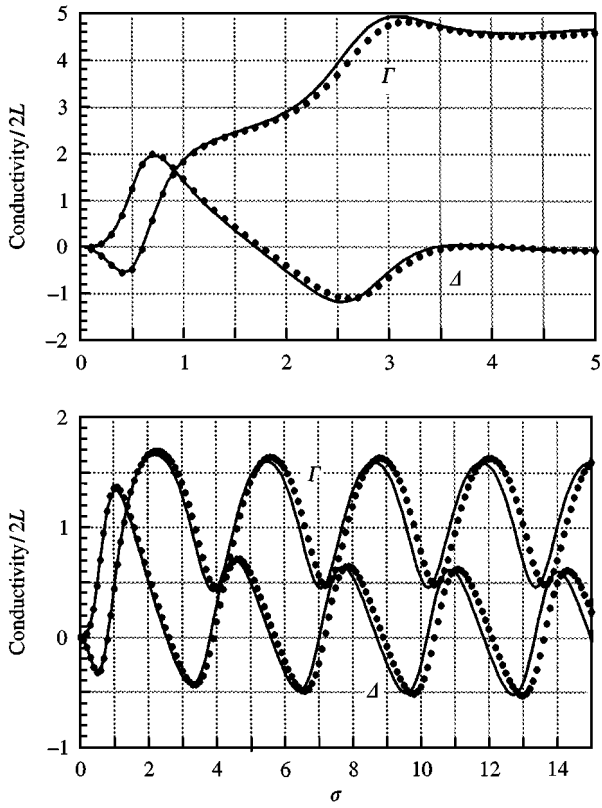

Figure 13. Rayleigh conductivity for a square aperture with one-sided and equal two-sided grazing flow calculated with the three-dimensional numerical method (dotted line) and the approximate theory (solid line).

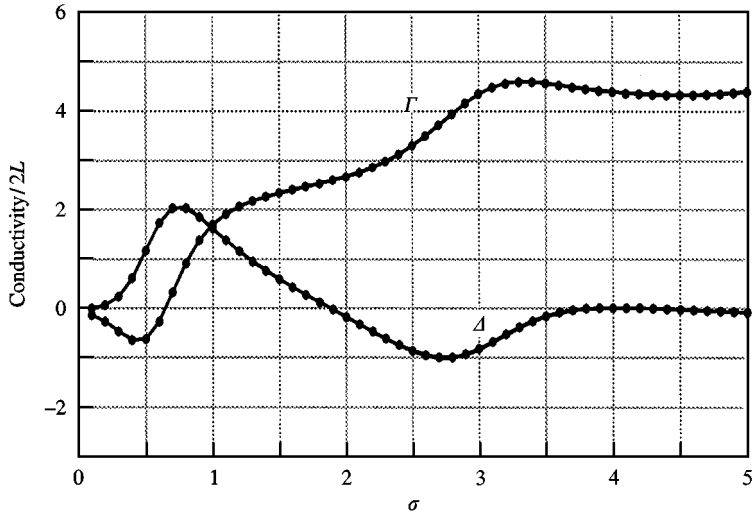

Figure 14. Rayleigh conductivity for one sided grazing flow past the crown shaped aperture. Comparison of results for serrated edge at the leading edge (solid line) and serrated edge at the trailing edge (dots).

the vortex sheet displacement on the spanwise coordinate x_3. The integro-differential equation (2.8) can then be simplified by explicitly performing the integration on the right-hand side with respect to y_3. When the equation is also integrated with respect to x_3 over the span, the analog of equation (2.12) assumes the one-dimensional form

$$\int_{-1}^{1} Z'(Y_1)[\ln|Y_1 - X_1| + \mathscr{L}(X_1, Y_1)]\,\mathrm{d}Y_1 + \lambda_1 \mathrm{e}^{\mathrm{i}\sigma_1 X_1} + \lambda_2 {}^{\mathrm{i}\sigma_2 X_1} = 1, \quad |X_1| < 1, \quad (3.15)$$

where

$$Z' = \frac{-2\zeta\rho_0\sigma^2(U^+)^2}{\pi L(p_0^+ - p_0^-)},$$

$$\mathscr{L}(X_1, Y_1) = -\ln\{b/L + \sqrt{[(b/L)^2 + (X_1 - Y_1)^2]}\} + \sqrt{\{1 + (L/b)^2(X_1 - Y_1)^2\}} - (L/b)\,|X_1 - Y_1|;$$

$\lambda_{1,2}$ are constants to be determined, and b is the span.

Equation (3.15) is solved by collocation; the values of $\lambda_{1,2}$ are determined by imposing the Kutta condition at the upstream edge $X_1 = -1$ as before, and the conductivity is calculated from

$$K_R = -\frac{\pi b}{2}\int_{-1}^{1} Z'(Y_1)\,\mathrm{d}Y_1.$$

Predictions of $K_R(\omega)$ obtained in this way for a square aperture in one or two-sided grazing flow are plotted as solid curves in Figure 13. The dotted curves in Figure 13 correspond to the numerical solution of the full three-dimensional equation of motion (2.8) obtained with a discretization corresponding to 60 mesh elements in the streamwise direction for the one-sided flow case and 70 for the two-sided flow case. It is clear from the figure that the one-dimensional approximation produces a good prediction to the motion of the vortex sheet in the mouth of the square aperture. The approximation does not work as well for lower aspect ratio apertures nor for apertures with tapered spans.

4. REVERSE FLOW RECIPROCITY

Reverse flow reciprocity (Howe *et al.* 1996) requires that the Rayleigh conductivity at a given frequency ω be unchanged in value when the directions of the mean flows on both sides of the wall are reversed. The theorem has been verified in Section 3 for forward and backward facing triangular apertures.

More dramatic confirmation of the theorem is exhibited in Figure 14, where the conductivities for a square aperture with either a serrated leading or serrated trailing edge (the "crown") are seen to be identical. This conclusion may be very significant for the design of flow control devices that depend on the use of serrations to "break up" an organized flow in an attempt to minimize coherent generation of sound and vibration.

5. CONCLUSION

When a sound wave impinges on a wall aperture in the presence of high Reynolds number flow, there is generally an exchange of energy between the sound and the flow brought about by acoustically induced vortex shedding. For a small aperture, the motion in its immediate neighborhood can be regarded as incompressible, and the interaction with the sound is conveniently expressed in terms of the Rayleigh conductivity K_R.

In this paper $K_R(\omega)$ has been computed for a variety of apertures in a wall of infinitesimal thickness in the presence of high Reynolds number grazing flow. The shear layer in the aperture is modelled by a linearly disturbed vortex sheet. For one-sided flow over apertures with equal maximum streamwise dimension, the Strouhal number range in which energy in extracted from the mean flow is found not to vary significantly with aperture shape. The centre of this range corresponds approximately to the frequency of the lowest order "operating stage" of self-sustained (*unforced*) oscillations of the aperture shear layer, which is therefore effectively independent of aperture shape.

Self-sustaining oscillations cannot occur in the ideal limit of a wall of zero thickness when the flows are the same on both sides, although forced motion by an incident disturbance can still induce vortex shedding and a positive or negative exchange of energy with the mean flow. In such cases, $K_R(\omega)$ becomes essentially periodic when the Strouhal number exceeds about 3, and the number of distinct values taken by the maxima or minima of the real and imaginary parts of K_R turns out to be equal to the number of distinct streamwise length scales that characterize aperture geometry.

The reverse flow reciprocal theorem requires the value of $K_R(\omega)$ to be unchanged when the mean flow directions of both sides of the wall are reversed. This is confirmed by our computations, and is remarkable because the edges of the aperture at which vorticity is generated and on which vorticity impinges are reversed in the reciprocal problem, and the respective geometries of these cases can be markedly different.

ACKNOWLEDGEMENTS

The authors gratefully acknowledge the valuable assistance of Kadin Tseng of the Boston ted by the Air Force Office of Scientific Research under Grant No. F49620-96-1-0098 administered by Major Brian Senders.

REFERENCES

BLAKE, W. K. & POWELL, A. 1986 *The Development of Contemporary Views of Flow-tone Generation*, pp. 247–315. New York: Springer-Verlag.

CHANAUD, R. C. 1994 Effects of geometry on the resonance frequency of Helmholtz resonators. *Journal of Sound and Vibration* **178,** 337–348.

HILDEBRAND, F. B. 1976 *Advanced Calculus for Applications*, p. 301. Englewood Cliffs, NJ: Prentice-Hall.

HOLGER, D. K., WILSON, T. A. & BEAVERS, G. S. 1977 Fluid mechanics of the edgetone. *Journal of the Acoustical Society of America* **62,** 1116–1128.

HOWE, M. S. 1981*a* The influence of mean shear on unsteady aperture flow, with application to acoustical diffraction and self-sustained cavity oscillations. *Journal of Fluid Mechanics* **109,** 125–146.

HOWE, M. S. 1981*b* On the theory of unsteady shearing flow over a slot. *Philosophical Transactions of the Royal Society of London*, **A-303,** 151–180.

HOWE, M. S. 1997*a* Edge, cavity and aperture tones at very low Mach numbers. *Journal of Fluid Mechanics* **330,** 61–84.

HOWE, M. S. 1997*b* Influence of wall thickness on Rayleigh conductivity and flow-induced aperture tones. *Journal of Fluids and Structures* **11,** 351–366

HOWE, M. S. 1997*c* Low Strouhal number instabilities of flow over apertures and wall cavities. *Journal of the Acoustical Society of America* **102,** 772–780.

HOWE, M. S., SCOTT, M. I. & SIPCIC, S. R. 1996 The influence of tangential mean flow on the Rayleigh conductivity of an aperture. *Proceedings of the Royal Society of London* A**452,** 2303–2317.

LAMB, S. H. 1932 *Hydrodynamnics*, 6th, reprinted 1995 edition, p. 373 Cambridge: Cambridge University Press.

PIERCE, A. D. 1989 *Acoustics*: *An Introduction to its Phsical Principles and Applications*. The Acoustical Society of America.

POWELL, A. 1961 On the edgetone. *Journal of the Acoustical Society of America* **33,** 395–409.

RAYLEIGH, J. W. S. 1945 *The Theory of Sound*, Vol. II, p. 173, New York: Dover Publications.

ROCKWELL, D. 1983 Oscillations of impinging shear layers. *AIAA Journal* **21,** 645–664.

ROSSITER, J. E. 1964 Wind tunnel experiments of the flow over rectangular cavities at subsonic and transonic speeds. Technical Report 3438, Aeronautical Research Council Reports and Memoranda.

SCOTT, M. I. 1995 The Rayleigh conductivity of a circular aperture in the presence of a grazing flow. Master's thesis, Boston University.